JOURNAL OF GEOPHYSICAL RESEARCH, VOL. 94, NO. C8, PAGES 10,921–10,935, AUGUST 15, 1989

A Two-Dimensional Coupled Ice-Ocean Model of the Bering Sea Marginal Ice Zone

LAKSHMI H. KANTHA[1] AND GEORGE L. MELLOR

Atmospheric and Oceanic Sciences Program, Princeton University, Princeton, New Jersey

A two-dimensional coupled ice-ocean model has been formulated and applied to the wintertime Bering Sea marginal ice zone. The oceanic component is a multilevel model that incorporates second-moment closure for turbulent mixing in the water column. The ice cover is modeled as a viscous-plastic continuum. Melting at the ice-ocean interface is computed using well-known law-of-the-wall concepts in a turbulent boundary layer, with particular attention to the disparate momentum and scalar transfer resistance coefficients over rough walls. The thermodynamic and dynamical interactions between the ocean and the ice cover and the energy balances at the air-ice and air-sea interfaces are modeled according to the companion paper (Mellor and Kantha, this issue). The model incorporates barotropic tides, both diurnal and semidiurnal, for application to the Bering Shelf. Double-diffusive fluxes across the interface between the colder, fresher layer beneath the melting ice and the warmer, more saline water underneath are prescribed from laboratory data on double-diffusive convection. During winter, sea ice in the central Bering Sea is transported toward the shelf break by off-ice winds, where it encounters northward flowing warmer north Pacific waters and melts. It is this situation to which the two-dimensional model has been applied by neglecting all variations in the along-ice-edge direction. The water conditions downstream of the ice edge, the ice conditions upstream, and the wind stress are the primary inputs to the model. The model simulates transition from ice-covered to open ocean conditions and the associated ice edge front and the two-layer circulation underneath the ice cover. Sensitivity studies indicate that the density structure and the circulation beneath the ice and the position of the ice edge are rather sensitive to the parameters affecting the dynamics and the thermodynamics of the coupled ice-ocean system. Even small changes in the relevant parameters can cause a substantial retreat or advance of the ice edge, which may help explain why marginal ice zones are such dynamically active regions.

1. INTRODUCTION

Marginal ice zones (MIZs) are regions of the world's oceans where the ice cover gives way to open water. They are dynamic regions, profoundly influenced by the interaction of all three mediums: the ice, the ocean, and the atmosphere. Their variability on synoptic time scales is important for numerous ice edge processes associated with MIZs, such as ice edge fronts, meanders, and mesoscale eddies. MIZs are important to our understanding of climatic fluctuations as well.

The ice cover mediates the interaction between the atmosphere and the ocean in a MIZ, and therefore the influence of ice cover is rather crucial to the dynamics and thermodynamics of the coupled system as a whole. In this article, however, we will deal only with the coupled ice-ocean medium, wherein the atmospheric forcing is prescribed and unaffected by the changes in the ice-ocean system.

The ultimate objective of the current study and the companion study by *Mellor and Kantha* [this issue] (hereinafter MK) is the development of a general purpose coupled ice-ocean model with realistic dynamical and thermodynamic coupling between the two media, simple but plausible ice rheology, and a fully three-dimensional multilevel ocean general circulation model subcomponent for proper parameterization of ice-ocean interactions. Our goal is a model that is suitable for simulation of local ice edge processes in a MIZ as well as the circulation in a large ice-covered ocean body such as the Arctic under the most general conditions. The one-dimensional studies of MK was the first step in the process of evaluation of the various subcomponents of the model, whereas the central Bering Sea MIZ simulation presented here is an intermediate step.

Coupled ice-ocean models have been applied to MIZ processes in the past, notable examples being *Roed and O'Brien* [1983], *Roed* [1984], *Smedstad and Roed* [1985], and *Hakkinen* [1986*a*, *b*]. These authors attempted to simulate and understand ice edge processes such as upwelling/downwelling, ice banding, and eddy generation, using the simplest possible dynamics. Thus they restricted the oceanic component to a reduced gravity model and concentrated on the ice-ocean interaction, using either simplified [*Roed and O'Brien*, 1983] or comprehensive [*Hakkinen*, 1986*a*, *b*] ice rheology. On the other hand, multilevel ocean models have been coupled to the ice and applied to the Arctic Ocean by *Hibler and Bryan* [1987] and *Semtner* [1987] and to a wind-driven coastal shelf by *Ikeda* [1985]. These authors used Hibler's viscous plastic ice rheology to model internal ice stresses [*Hibler*, 1979]. *Semtner* [1987] has used simplified Hibler rheology. None of these, however, tried to model the turbulent exchange processes, at the ice-ocean interface, that involve disparate heat and salt resistance coefficients.

Some studies have concentrated on the thermodynamic effects of sea ice cover [e.g., *Parkinson and Washington*, 1979], assuming the fluxes at the ice-ocean interface as prescribed a priori. On the other hand, *Hibler and Walsh* [1982] and *Lepparanta and Hibler* [1985] have concentrated on the ice dynamics, ignoring the thermodynamical interaction completely.

It is only recently that the disparity in the various under-

[1]Now at Institute for Naval Oceanography, Stennis Space Center, Mississippi.

Copyright 1989 by the American Geophysical Union.

Paper number 89JC00899.
0148-0227/89/89JC-00899$05.00

ice resistance coefficients has been taken into account, starting with *Mellor et al.* [1986], who formulated a one-dimensional multilevel model of the ocean and coupled it to the ice thermodynamically. *Ikeda* [1986] also formulated a similar one-dimensional model, with a somewhat simpler second-moment closure, but he ignored the disparity in the momentum and scalar resistance coefficients. This approach has some drawbacks. For example, considering the heat and salt resistance coefficients under ice to be the same does not lead to constitutional supercooling during freezing conditions, a phenomenon that could be of considerable importance in the formation of frazil ice [*Steele et al.*, 1989].

A two-dimensional (in the vertical plane) version of the ice-ocean coupled model under development is applied in this study to simulate the central portion of the wintertime Bering Sea MIZ. During winter, sea ice in the Bering Sea is formed in the northern regions of the inner shelf and transported southward toward the shelf break by off-ice winds, where it encounters the generally northward flowing warmer north Pacific Ocean waters and melts. Following the analysis of *Hendricks et al.* [1985], all variations in the along-ice-edge direction are neglected, so that a two-dimensional model simulating changes across the ice edge can be applied. This presumes that the along-ice-edge scales are much larger than the scales across the ice edge, a condition often approximated in a MIZ.

On the Bering Sea shelf the ice is generated in the northern regions mainly in polynyas near coastal regions during offshore wind conditions and transported toward the outer shelf by winds. It would take a fully three-dimensional model of the Bering Shelf to reproduce these ice generation aspects and the circulation on the shelf. However, our focus in this work is rather limited. We pose the following question: Given a certain ice influx onto the outer shelf, how then does the ice edge position behave as a function of the various forcing parameters? Essentially, this is another way of inquiring into the influence of forcing parameters on the melting rate of ice. This question can be answered using a local two-dimensional model, and the need to use a three-dimensional model to incorporate the complexities of ice generation and shelf circulation does not arise.

The primary model inputs are the water properties downstream (southward) of the ice edge, the ice properties upstream, and the wind velocity. The latter is assumed to be uniform over the MIZ, although the atmospheric boundary layer itself is known to undergo significant changes across a MIZ because of the differing roughness scales associated with the interior pack ice, rafted floes in the MIZ, and open water, as well as of the differing net heat exchange between the ocean and the atmosphere in these regions (see for example, *Overland et al.* [1983], *Reynolds* [1984], *Bennett* [1986], and *Kantha and Mellor* [1989]). To account for these changes, however, a coupled ice-ocean-atmosphere model is needed, and this is beyond the scope of this paper. Numerical simulation of the modifications undergone by the atmospheric boundary layer as it traverses the marginal ice zone is the subject of *Kantha and Mellor* [1989]. The results from coupling this two-dimensional boundary layer model with the ice-ocean model described in this paper will be the subject of a future paper.

The model simulates the transition from ice cover to open ocean and the associated ice edge front and two-layer circulation underneath the ice cover. The oceanic component is a multilevel model that solves the primitive equations of motion and incorporates, as well, a second-moment closure for vertical turbulent mixing in the water column. The latter parameterizes turbulent mixing under strong buoyancy fluxes at the sea surface, due to input of less saline water by melting ice and brine rejection during freezing. The associated heat and salt exchanges at the ice-ocean interface are computed using well-known law-of-the-wall concepts in a turbulent boundary layer over a rough surface. The disparity in resistance coefficients for momentum, heat, and salt in a turbulent flow over a rough surface in the momentum, heat, and salt flux formulations is an important aspect of the model. The model uses the *Yaglom and Kader* [1974] formulation for heat and mass transfer over a rough wall instead of the *Sheppard* [1958] formulation used by *Mellor et al.* [1986]. Treatment of the thermodynamic interaction between the ice and the ocean also accounts for the energy balance at the air-sea interface as well as that at the air-ocean interface in the leads between ice floes.

The dynamical interaction between the ice and the ocean is accomplished through the solution of continuity equations for the areal fraction and mean thickness of ice and momentum equations that include the effect of the Coriolis force, the applied wind stress, the shear stress at the ice-ocean interface, and the internal ice stresses. The ice cover in the MIZ is modeled as a viscous-plastic continuum following *Hibler* [1979] and *Lepparanta and Hibler* [1985]. With our goal of development of a general ice-ocean coupled model in mind, the internal ice stress terms are retained in the formulation, although they are not always important in the MIZ, as, for example, during off-ice wind conditions.

The melting ice in a MIZ produces a two-layer stratification underneath, with cooler fresher water masses overlying saltier warmer masses, a condition conducive to double-diffusive exchange of heat and salt between the two layers [*Huppert and Turner*, 1981; *Turner*, 1985]. Such fluxes across the interface between the layers lead to enhanced mixing in both layers and could cause considerable transfer of heat from the lower to the upper layer. In fact, *Hendricks et al.* [1985] imply that double diffusion is an important component of heat balance in a MIZ. A better understanding of the importance of double-diffusive transfer to ice melting in a MIZ is also a goal of this study. Double-diffusive fluxes are therefore included in the model and parameterized from laboratory data on double-diffusive convection by *Marmorino and Caldwell* [1976] and *Takao and Narusawa* [1980].

Tidal (and inertial) motions on a shelf are an important source of mixing, especially in the bottom layers. In this study we are interested in the wintertime MIZ observations by *Hendricks et al.* [1985] and *Muench and Schumacher* [1985] on a line across the Bering shelf in the vicinity of St. Matthew Island. Tidal measurements also were made by *Mofjeld* [1986] in the vicinity of this line. The model incorporates barotropic tides with tidal forcing prescribed from observational data cited by Mofjeld. Both diurnal and semidiurnal tides are prescribed, although on the Bering shelf, diurnal constituents are by far the more important in its outer reaches [see *Mofjeld*, 1986].

The primary goal of this study is to explore the causes of variability in a MIZ. In particular, we would like to examine, for example, the relative importance of tidal, wind-induced and double-diffusive mixing and the effect of heat loss

through the leads on the rate of melting of ice. The strategy is to obtain a base case simulation of the central portion of the wintertime Bering Sea MIZ, using the observations of Hendricks et al. as a guide, and then to investigate the changes in the ice edge position and the circulation underneath that is brought on by changes in the various parameters governing the different processes that affect its variability.

The paper is organized as follows: Section 2 deals with the formulation of the ice dynamics component of the coupled ice-ocean model. The rest of the details of the coupled model can be found in the companion paper by MK. Section 3 deals with simulation of the wintertime Bering Sea MIZ and sensitivity studies that elaborate on the dependence of the ice edge position and the circulation underneath the ice on various model parameters. Section 4 contains concluding remarks.

2. Model Formulation

The coupled model consists of a primitive equation, multilevel, fully nonlinear ocean model that interacts with an ice model which is similar to the lowest resolution ice model of *Semtner* [1976] but which differs in the manner in which several processes are physically modeled. The details of the coupled model can be found in the paper by MK. Only some salient aspects and features specific to this study will be repeated here. The companion paper (MK) does not describe the constitutive equation for internal ice stresses, which will therefore be described here for completeness and future reference, even though the internal ice stresses are not important in the present application, which deals with off-ice winds in a MIZ. The ice is pretty much in free drift under these conditions. However, the compaction that takes place during on-ice winds in a MIZ would require inclusion of internal ice stresses.

The most important feature of the coupled model is the careful treatment of the turbulent exchange processes at the ice-ocean interface. Particular attention is given to the molecular sublayer embedded inside the roughness elements in the turbulent boundary layer underneath the ice. The turbulent mixing itself is parameterized by *Mellor and Yamada*'s [1982] level 2 1/2 model. Since experimental evidence suggests that the size of the eddies that participate in the turbulence cascade process is limited by stable stratification, we impose an upper bound of 0.5 q/N on the turbulence length scale l, where q is the turbulence velocity and N is the ambient buoyancy frequency.

2.1. *Ice Model*

An important attribute of ice cover is the presence of relatively ice-free open areas through which a large part of the heat exchange between the ocean and the atmosphere takes place. It is therefore important to keep track of the extent of "ice-free" regions. This is done by writing a conservation equation for the areal fraction of ice. This empirical equation along with mass and momentum conservation equations describe the dynamics of ice cover:

$$\frac{\partial}{\partial t}(A) + \frac{\partial}{\partial x_i}(AU_{Ii}) = \frac{\rho_0}{\rho_I}\left[\Phi(1-A)W_{AO}\frac{A}{D_I}\right] + H_A \qquad (1)$$

$$0 \le A \le 1$$

$$\frac{\partial}{\partial t}(D_I) + \frac{\partial}{\partial x_i}(D_I U_{Ii}) = \frac{\rho_0}{\rho_I}[(1-A)W_{AO} + A(W_{AI} + W_{IO})] + H_D \qquad (2)$$

$$\frac{\partial}{\partial t}(D_I U_{Ij}) + \frac{\partial}{\partial x_i}(D_I U_{Ii} U_{Ij}) - \varepsilon_{ijk} f_i D_I U_{Ik} = -gD_I \frac{\partial}{\partial x_i}(\zeta) + \frac{A}{\rho_I}(\tau_{AIj} - \tau_{IOj}) + \frac{1}{\rho_I}\frac{\partial}{\partial x_i}(\sigma_{ij}) \qquad (3)$$

The first term on the right-hand side of (3) denotes the pressure gradient due to sea surface slope [*Hibler*, 1979; *Parkinson and Washington*, 1979], the second term denotes the stresses at the air-ice and ice-ocean interfaces, and the last term denotes the internal ice stresses. The quantities A, D_I ($= Ah_I$), and U_I denote the areal concentration of ice, the ice volume per unit area, and the velocity of ice (see MK for the definition of the other quantities).

Considerable empiricism is involved in modeling the internal stress terms. It is widely known that ice cover cannot be modeled correctly as a Newtonian viscous fluid and that ice can flow plastically and can stand compression well but not tension. However, the choice of the best rheology for the MIZ is not clear. *Shen et al.* [1987] indicate that while a plastic rheology might be a good approximation for a closely packed collection of large ice floes, interlocking with and grinding against one another, a situation extant in the interior Arctic Pack ice, for a MIZ, where a loose collection of relatively widely spaced small ice floes bump and grind against one another, the rheology might more appropriately be a non-Newtonian fluid rheology [*Shen et al.*, 1987]. Such collisional rheology has been modeled by these authors in terms of a collection of uniformly sized circular disks. However, there are unresolved issues related to the transition between the two rheologies. Therefore for the time being we will adopt the conventional practice and follow *Hibler* [1979] in considering the ice to be a viscous-plastic isotropic continuum. The ice dynamics model will therefore be primarily applicable to relatively dense ice pack conditions. However, this is of little consequence to the current application because under off-ice winds of primary concern in this paper the ice concentration seldom becomes large enough for significant buildup of internal ice stresses. Ice stresses are included here primarily for completeness and future reference.

The constitutive law for ice can therefore be written as

$$\sigma_{ij} = 2\eta_0 \varepsilon_{ij} + \left[(\zeta_0 - \eta_0)\varepsilon_{kk} - \frac{P_I}{2}\right]\delta_{ij} \qquad (4)$$

where η_0 is the shear viscosity, ζ_0 is the bulk viscosity, and P_I is the pressure (ice strength) term, which are given by

$$P_I = P^* D_I \exp[-C(1-A)] \qquad (5)$$

$$\zeta_0 = \frac{P_I}{2\Delta} \qquad (6)$$

$$\eta_0 = \frac{P_I}{2\Delta e^2} \qquad (7)$$

The quantity ε_{ij} is the strain rate (deformation) tensor $\equiv 0.5$ $(\partial U_I/\partial X_j + \partial U_{Ij}/\partial X_i)$ and

$$\Delta = \max\left\{\left[\varepsilon_{kk}^2 + \frac{1}{e^2}(2\varepsilon_{ij}\varepsilon_{ij} - \varepsilon_{kk}^2)\right]^{1/2}, \varepsilon_0\right\} \quad (8)$$

The quantity e is the ratio of compressive to shear strengths, that is, the ratio of the major to minor axes of the elliptical yield curve in the principal stress space. *Hibler* [1979] sets $P^* = 5 \times 10^3$ N m^{-2}, $C = 20$, $e = 2$, and $\varepsilon_0 = 2 \times 10^{-7}$ s^{-1}. The value of e determines the relative importance of the bulk and shear viscosities. For $e \to \infty$ the shear viscosity vanishes.

The above formulation renders the ice a plastic medium for which the internal stresses become independent of the strain rates where the rates are large. However, when the strain rates are small, a Newtonian viscous behavior is retained. The yield curve is an ellipse in the principal stress space, almost wholly confined to the negative region, so that the ice strength is mainly compressive and very small in tension [see *Hibler*, 1979; *Lepparanta and Hibler*, 1985].

Hakkinen [1986*a*, *b*] used a constitutive law, which can also be written in the form of equation (5) but with $\eta = P_I/2\tilde{\Delta}$ and $\zeta = 0$, where $\tilde{\Delta}$ is a function of the two invariants of ε_{ij}:

$$\tilde{\Delta} \equiv \exp\left(-1.5 \times 10^8 \varepsilon_{kk}|\varepsilon_{kk}^2 - \varepsilon_{ij}\varepsilon_{ij}|\right) \quad (9)$$

Hakkinen also chose a value for P^* that is significantly smaller than Hibler's value and puts $C = 15$ instead of 20. Her formulation provides lesser resistance of ice to compression, no tensile strength, and no bulk viscosity.

Roed and O'Brien [1983] used only the pressure term ($\eta_0 = \zeta_0 = 0$) for model simulations in a marginal ice zone. *Semtner* [1987] used the bulk viscosity limit of Hibler's formulation ($\eta_0 = 0$) in his long-term simulation of the Arctic ice. This simple limit relaxes the strong time step constraints imposed by the full formulation so that long-term integrations are feasible. However, since these simpler formulations have limited domains of validity, it is preferable to retain the full rheology for general applicability.

All the above rheological formulations postulate ice strength that is proportional to the ice thickness. More recently, for mesoscale coastal problems, *Overland and Pease* [1988] have argued for an ice strength that is proportional to the square of the ice thickness.

In this study all variations in the along-ice-edge direction are ignored, and the governing equations for ice therefore become substantially simpler. For convenience, the y coordinate is aligned with the ice edge. Therefore the equations can be written in component form as

$$\frac{\partial}{\partial t}(A) + \frac{\partial}{\partial x}(AU_I) = \frac{\rho_0}{\rho_I}\left[\Phi(1-A)\frac{W_{AO}}{h_I}\right] + H_A \quad (10)$$

$$0 \le A \le 1$$

$$\frac{\partial}{\partial t}(D_I) + \frac{\partial}{\partial x}(D_I U_I) = \frac{\rho_0}{\rho_I}[(1-A)W_{AO} + A(W_{AI} + W_{AO})] + H_D \quad (11)$$

$$\frac{\partial}{\partial t}(D_I U_I) + \frac{\partial}{\partial x}(D_I U_I U_I) - fV_I D_I = -gD_I\frac{\partial \zeta}{\partial x} + \frac{A}{\rho_I}(\tau_{AIx} - \tau_{IOx}) + F_{Ix} \quad (12)$$

$$\frac{\partial}{\partial t}(D_I V_I) + \frac{\partial}{\partial x}(D_I U_I V_I) + fU_I D_I = -gD_I\frac{\partial \zeta}{\partial y} + \frac{A}{\rho_I}(\tau_{AIy} - \tau_{IOy}) + F_{Iy} \quad (13)$$

where

$$F_{Ix} = \frac{1}{\rho_I}\frac{\partial}{\partial x}\left[(\eta_0 + \zeta_0)\frac{\partial U_I}{\partial x} - \frac{P_I}{2}\right] \quad (14)$$

$$F_{Iy} = \frac{1}{\rho_I}\frac{\partial}{\partial x}\left[\eta_0\frac{\partial V_I}{\partial x}\right] \quad (15)$$

Equations (10)–(15), along with equations (4)–(8), are solved for four prognostic quantities: ice concentration A, ice volume per unit area D_I, and the components of ice velocity U_I, and V_I. Note that Φ is an empirical constant which is assigned different values for melting and freezing situations, Φ_M and Φ_F. The evaluation of the source/sink terms in the continuity equations (W_{AO}, W_{AI}) and of the shear stress terms (τ_{AI}, τ_{AO}) in these equations are discussed by MK. A few remarks on the source/sink terms are, however, in order here.

In application to a MIZ we are primarily concerned with melting conditions at the ice-ocean interface. The process of ice melting in a MIZ is rather complex. A variety of processes are at play, including bottom and lateral ablative processes, the relative importance depending on a variety of factors including floe size. Eddy activity, wave action, and collisional fracture of floes also enhance melting at the ice edge [*Josberger*, 1987]. It is clearly difficult to incorporate all these processes. *Maykut and Perovich* [1987] have recently reexamined the question of lateral melting of ice floes due to heat input to the leads. They point out that assuming all the excess heat in the leads goes to melt the ice floes laterally is one of the limits. This is equivalent to setting $\Phi_M = 1$ in (10). In this study we put $\Phi_M = 0.5$ and $\Phi_F = 4$ over the entire MIZ in accordance with the findings of MK.

Horizontal diffusion terms H_A and H_D on the right-hand sides of (10) and (11) are necessary for numerical reasons. *Hibler* [1979] used both biharmonic and harmonic diffusion terms, while *Hakkinen* [1986*a*] used a "weak" Laplacian term of unspecified magnitude. The diffusion terms can be written as

$$H_A = A_D\nabla^2 A - A_{DB}\nabla^4 A$$
$$H_D = A_D\nabla^2 D_I - A_{DB}\nabla^4 D_I \quad (16)$$

where A_D and A_{DB} are coefficients of harmonic and biharmonic diffusion. *Hibler* [1979] prescribes values for A_D and A_{DB} corresponding to a cell Reynolds Number R_c of about 10 (assuming a typical ice velocity of 4 cm s^{-1}), where R_c is $U_I\Delta X/A_D$ for harmonic and $U_I\Delta X^3/A_{DB}$ for biharmonic diffusion.

Biharmonic diffusion is efficient in damping out high wave number numerical noise in the interior of a field, whereas a Laplacian diffusion appears to be essential for damping out oscillations in regions of strong gradients (such as an ice edge). In this work, which essentially deals with a marginal zone, we have put $A_{DB} = 0$ and used a value of A_D corresponding to a value of about 4 for the cell Reynolds Number R_c. This is not much different from the total effective diffusion employed by *Hibler* [1979]. It can be

shown that this is the value needed to damp out oscillations behind a propagating front governed by an advection-diffusion equation (see *Rood* [1987] for a comprehensive discussion of the advection-diffusion equation and its solution).

2.2. *Coupling Between the Ice and the Ocean*

The dynamical and thermodynamic coupling between the ice and the ocean is described in detail by MK. In this work, following *Overland et al.* [1983] and *Overland* [1985], we set the drag coefficient at the air-ocean interface C_{DAO} to 2×10^{-3} and that at the air-ice interface C_{DAI} to 3.8×10^{-3}. These values are appropriate to a MIZ.

Some comments with respect to the momentum roughness scale z_0 and the Yaglom-Kader formulation are in order. In this formulation (see MK) the law of the wall for heat transfer over a rough surface at high Prandtl numbers can be written as

$$T_w - T(z) = T_* \left[\frac{Pr_t}{k} \ln \left(-\frac{z}{z_0} \right) + B_T \right] \tag{17}$$

where

$$B_T = b(\nu/\alpha_T)^{0.66}(u_\tau z_0/\nu)^{0.5}$$

u_τ is the friction velocity, ν the kinematic viscosity, and α the molecular diffusivity. The quantity T_W denotes the temperature at the wall, and $T(z)$ refers to temperature at distance z from the wall. T_* is the friction temperature, Pr_t is the turbulent Prandtl number, and k is the von Karman constant. A similar relation holds for salinity. *Yaglom and Kader* [1974] recommended a value of 3.14 for b, and this is also the value used by *Steele et al.* [1989]. However, *McPhee et al.* [1987], in a careful study of observational data on melting in the Greenland Sea MIZ, found that a value of $b = 1.57$ provided the best agreement on melting rates. Nevertheless, it is not clear what the correct value of b should be. Josberger's observations [*Josberger*, 1987] appear to correspond to a value of b that is about one-fourth the Yaglom and Kader value (M. G. McPhee, personal communication, 1988). Our own simulations, as we will see shortly, suggest a still smaller value for b. The issue is, however, complicated by uncertainties in the estimation of the under-ice roughness scale z_0. The formulation therefore needs to be studied further. Nevertheless, the fact that the resistance coefficients to momentum, heat, and salt exchanges across a rough under-ice surface are significantly different and that this exerts considerable influence on these exchanges is well corroborated by empirical evidence.

It is worth noting at this point that the Yaglom and Kader formulation is a semiempirical fit to laboratory observational data on turbulent heat and mass exchanges across a rough surface. It is also somewhat similar to *Owen and Thompson* [1963] and *Dipprey and Sabersky* [1963] formulae, although the exponents and the constants differ. However, although the formulation is well supported at moderate values of Prandtl number ν/α_T, representative of heat transfer in water ($Pr \sim 13$), its empirical basis is less firm at very high values of Schmidt number ν/α_S, represented by salt transfer ($Sc \sim 2400$). The reason is that even though there are a few experiments on ion exchanges at a rough surface representative of such Schmidt numbers [*Dawson and Trass*, 1972; *Grifoll et al.*, 1986] and the data from one of these has been used in Yaglom and Kader formulation, these experiments are for two-dimensional roughness elements. No laboratory experiments appear to have been done for three-dimensional roughness elements at high Schmidt numbers.

The corresponding relation for turbulent heat (and salt) transfer across a smooth surface at high Prandtl (Schmidt) numbers is [*Kader and Yaglom*, 1977]

$$T_w - T(z) = T_* \left[\frac{Pr_t}{k} \ln \left(-\frac{u_\tau z}{\nu} \right) + B_L \right] \tag{18}$$

where

$$B_L = 12.5\ (\nu/\alpha_T)^{0.66} - 6.0$$

This provides the lower bound on heat and mass transfer, since toward the ice edge in a MIZ the ice thickness and therefore the under-ice roughness could become small enough for the ice surface to be considered hydraulically smooth.

The momentum roughness scale z_0 is modeled by MK as the weighted mean of ice-covered and ice-free regions, following *Taylor* [1987]:

$$z_0 = (z_{0I})^A (z_{0O})^{(1-A)} \tag{19}$$

where z_{0I} is the roughness scale of the undersurface of the ice and z_{0O} is the roughness scale of the ice-free region, taken from Charnock's relation $z_{0O} = 8.7\ u_\tau^2/g$, where we assume that the roughness obtained for the airside of the interface equals that for the waterside. However, it is not clear what the effective z_0 distribution across the MIZ should be. In the interior, where the leads are small and ice floes not rafted, the major contribution should be from the ice cover. And toward the edge of the MIZ the open water fraction becomes larger and the ice roughness decreases, so that the effective roughness might be expected to be weighted toward the open water. On the other hand, the ice floes toward the edge of the MIZ are increasingly buffeted by swell, and rafted, so that the effective z_0 might actually be larger. In view of this uncertainty, in most of this work we have assigned a constant value for z_0 across the MIZ. We do investigate the sensitivity of the results to Taylor's formulation.

There are also some minor departures from MK in this study. For simplicity, snow cover is ignored but snow albedo is used at the top of the ice cover. However, as by MK, the effective heat conductivity of ice is set to 1.5 times its usual value ($G = 1.5$) to account for the predominance of heat loss through thinner portions of the ensemble of ice thicknesses that are represented here by a single average thickness. The energy balances are explicitly computed at both the air-sea and air-ice interfaces (see Appendix A of MK). When the energy balance indicates an ice surface temperature above the freezing point (0°C), it is set equal to the freezing value, and the excess heat is used to melt ice at the top of the floe. This meltwater is immediately allowed to run off into the ocean, that is, the parameter h_{SW} as defined by MK is set to zero.

2.3. *Turbulent Mixing Beneath the Ice*

The three major sources of turbulent mixing beneath melting ice in a MIZ are (1) the shear stress at the ocean surface due to the action of the wind and ice drift, (2) the shear stress at the bottom of the shelf due to mean motion,

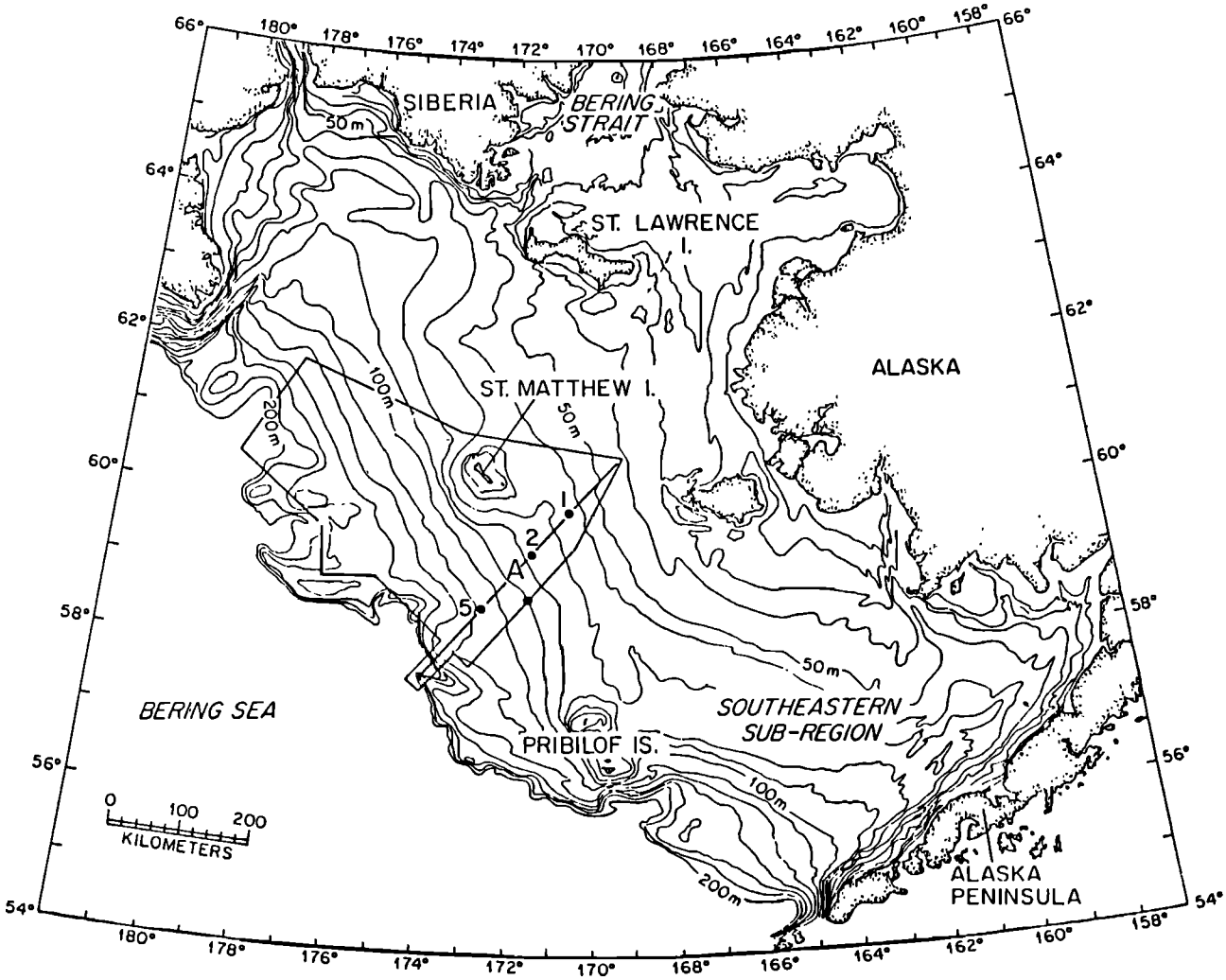

Fig. 1. A map of the Bering Sea showing the deployment of current meter moorings [from *Hendricks et al.*, 1985]. The model simulates conditions along the mooring transect.

tides, and inertial oscillations and (3) double-diffusive convection across the interface separating the upper fresher and colder layer from the layer below. Of these the tidal mixing and double diffusion require further elaboration.

Tidal forcing. Observations of tides on the Bering Sea shelf [*Mofjeld*, 1986] indicate their highly complex nature. The tides enter the outer shelf from the Pacific Ocean through the Aleutian Basin. The superinertial, semidiurnal components propagate freely across the shelf from the shelf break, while the subinertial diurnal components appear to be evanescent Sverdrup waves that decay across the shelf [*Mofjeld*, 1986]. The diurnal components dominate the outer shelf and are fairly uniform in the along shelf direction in the vicinity of St. Matthew Island [see *Mofjeld*, 1986, Tables 1 and 2], while the semidiurnal components become more important on the inner shelf. A composite of diurnal and semidiurnal tidal amplitudes of 28.4 and 22.6 cm appears to exist in the vicinity of the outer shelf, decreasing to 14.0 and 21.9 cm around the 50-m isobath (see *Mofjeld*, 1986, Table 4]. These observations are used to drive the model by modulation of the sea surface elevation at the ends of the x-z domain of the model shown in Figure 1.

Double-diffusive convection. Double-diffusive convection can contribute to a rapid vertical transfer of heat and salt in the oceans even when the water column is stably stratified in the mean. The process depends on the disparity in the molecular diffusivities of heat and salt. In the Bering Sea MIZ, in the presence of meltwater at the surface, the water layers immediately beneath the ice are fresher and colder than those closer to the bottom. This situation is conducive to double-diffusive convection [*Huppert and Turner*, 1981; *Turner*, 1985] which can transport heat and salt from the bottom layers to the vicinity of ice and therefore affect the melt rate of ice and the heat balance in the MIZ. *Hendricks et al.* [1985] considered double-diffusive transport to be an important component of the heat balance on the Bering sea shelf. It is our intention to investigate in this paper the relative contribution of this process to the melting of ice on the Bering Sea MIZ.

Some measurements of heat and salt transport across a double-diffusive interface have been made in the laboratory [e.g., *Marmorino and Caldwell*, 1976; *Takao and Narusawa*, 1980], and these observations are used to parameterize the heat and salt transport across the stable interface separating the two layers beneath the ice in the model. The expression

$$F_T = F^*\{4.38 \times 10^{-3}\tau_d^{-0.71}[4.6 \exp(-0.54(Tu - 1))]\} \quad (20)$$

gives the heat flux in W m^{-2} across a double-diffusive interface [*Takao and Narusawa*, 1980]. The Turner Number Tu and the parameter τ_d are

$$Tu = \beta_S \Delta S / \beta_T \Delta T \tag{21a}$$

$$\tau_d = \alpha_S / \alpha_T \tag{21b}$$

where ΔS and ΔT are the salinity and temperature differentials across the interface, and β_S and β_T are the corresponding coefficients of expansion $\beta_s \sim 8 \times 10^{-4}$ ppt^{-1}, $\beta_T \sim 4 \times 10^{-5}°C^{-1}$. The quantity τ_d, the ratio of molecular diffusivities of salt and heat, is taken as 0.0212. F^* is given in W m^{-2} by

$$F^* = 0.085\, k_T \left(\frac{g\beta_T \Delta T}{\nu \alpha_T}\right)^{0.33} \Delta T \tag{22}$$

where k_T is the heat conductivity [0.58 W $m^{-1}°C^{-1}$], ν is molecular diffusivity of momentum 1.8×10^{-6} m^2 s^{-1}, and α_T is the molecular diffusivity of heat 1.39×10^{-7} m^2 s^{-1}. The salt flux across the interface is given by

$$\rho C_p \frac{\beta_S F_s}{\beta_T E_T} = 0.034\, \tau_d^{-0.33} \tag{23}$$

where F_s is ppt m s^{-1}. For the values of constants cited above the kinematic heat and salt fluxes due to double-diffusive convection from the lower to the upper layer become

$$\langle wT \rangle^d = -1.381 \times 10^{-6} (\Delta T)^{4/3} \cdot \exp\{4.6 \exp[-0.54(Tu - 1)]\} \tag{24}$$

$$\langle wS \rangle^d = 0.01 \langle wT \rangle^d \tag{25}$$

the units of $\langle wT \rangle^d$ and $\langle wS \rangle^d$ being °C m s^{-1} and ppt m s^{-1}, respectively.

The above values are for double-diffusive convection occurring in isolation. There is no observational data for these fluxes in the presence of shear. A simple approximation is to assume that the double-diffusive fluxes can simply be added to other fluxes across the interface [see *Kantha*, 1986], and this practice is followed here. Note that τ_d must be nonunity for double diffusion to occur, and equation (20) is valid when

$$Tu > 0.49\, \tau_d^{-0.38} \tag{26}$$

2.4. *Boundary Conditions for the Model*

The boundary conditions applied at the ocean surface and the bottom have been discussed by MK. The lateral boundary conditions for the ice and ocean models are discussed here in the $x - z$ model context. We ignore density gradients in the y direction (parallel to the ice edge) by putting $\partial T/\partial y = \partial S/\partial y = \partial \rho/\partial y = 0$. This is consistent in the sense that the ice edge thermal front is along the ice edge, and therefore as long as the along-ice-edge scales are larger than those across, these conditions are well approximated. Thus the baroclinic component of currents is parallel to the ice edge. The y axis is oriented along the ice edge and is, in general, not parallel to the isobaths. And a constant nonzero along-ice-edge pressure gradient ($\partial \zeta/\partial y$) is imposed at the outer shelf. The sea surface elevation at the two ends of the model domain are prescribed as

$$\zeta(x = 0) = \zeta_{D0} \sin\left(\frac{2\pi t}{T_D}\right) + \zeta_{S0} \sin\left(\frac{2\pi t}{T_S} + \phi_0\right)$$

$$\zeta(x = L) = \Delta\zeta + \zeta_{DL} \sin\left(\frac{2\pi t}{T_D}\right) + \zeta_{SL} \sin\left(\frac{2\pi t}{T_S} + \phi_L\right) \tag{27}$$

where $x = 0$ denotes the outer shelf end of the model domain and $x = L$, the inner shelf end; $\Delta\zeta$ is the cross-shelf mean elevation change, T_D and T_S are the diurnal (23.93 hours) and semidiurnal (12.42 hours) tidal periods. The parameters ζ_{D0}, ζ_{S0}, ζ_{DL}, ζ_{SL}, ϕ_0, and ϕ_L are prescribed from Mofjeld's data: 28.4 cm, 22.6 cm, 14.0 cm, 21.9 cm, 136°, and 212°, respectively. A zero-gradient condition is used for both components of external mode (vertically averaged) velocity at both $x = 0$ and $x = L$.

As for internal mode quantities, a zero-gradient condition is imposed on the along-ice-edge velocity v and on the turbulence quantities at both $x = 0$ and $x = L$. The cross-ice-edge velocity component satisfies the Sommerfeld radiation condition

$$\frac{\partial u}{\partial t} + c \frac{\partial u}{\partial x} = 0 \qquad x = 0, L \tag{28}$$

where the phase speed c of the disturbances is computed at one grid point inward of the boundary. The finite differencing scheme is that due to *Orlanski* [1976]. Temperature and salinity at the boundaries are prescribed if they are being advected into the domain but advected out if the velocity is directed outward by solving

$$\frac{\partial}{\partial t}(T, S) + \frac{\partial}{\partial x}[u(T, S)] = 0 \tag{29}$$

From *Hendricks et al.* [1985] the prescribed temperature and salinity at $x = L$ are −1.7°C and 31.6 ppt, while those at $x = 0$ (near shelf break) are 2.5°C and 32.8 ppt. Since their measurements indicate a roughly barotropic condition near the shelf break, $\partial \zeta/\partial y$ is prescribed from

$$\frac{\partial \zeta}{\partial y} = -\frac{f}{g} U(x = 0) \tag{30}$$

$\Delta\zeta$ in (28) is prescribed from

$$\Delta\zeta = \frac{fL}{g} V(x = 0) \tag{31}$$

where $V(x = 0)$ is set to 8 cm s^{-1}.

For the ice model the inflow conditions on A, D_I, and U_I at $x = L$ are also prescribed from *Hendricks et al.* [1985] and zero-gradient conditions imposed at $x = 0$. At $x = L$, V_I is put to zero.

2.5. *Numerical Details*

We employ a finite difference formulation to solve the model equations presented above. The numerical grid is Arakawa C grid, where all quantities are at the center of the grid, with the exceptions of the u components of velocity of both water and ice, which are displaced half a grid interval to the west, and v components, displaced half a grid interval to the south. The bottom stresses are similarly staggered, whereas the stresses at the ocean surface are weighted means of ice-covered and ice-free quantities and therefore

conveniently centered on the grid. The shear stresses, vertical velocity component, and turbulence quantities are staggered in the vertical with respect to velocity, temperature, and salinity.

The time differencing is two-step leapfrog. The ocean component is solved explicitly in the horizontal (but implicitly in the vertical) using mode splitting and a time split of about 20. The ice component is solved implicitly to avoid stringent penalties in time step implied by potentially large internal ice stresses. The solution-splitting tendency associated with the computational mode in a leapfrog scheme is suppressed by the use of a time filter.

The numerical grid is 45 × 22, with a horizontal resolution of 7.5 km, a resolution that is rather too coarse to resolve some interesting ice edge processes such as ice banding but adequate for the present purposes. The grid covers the outer shelf with depths varying from 150 to roughly 50 m, and the bottom topography corresponds to that along the section shown in Figure 1, along which observations are available from the 1983 marginal ice zone experiment (MIZEX83).

The model is integrated from arbitrary homogeneous initial conditions until steady state conditions are reached. The ice edge features such as the sharp density front are therefore generated by the model and not prescribed a priori. An integration time of 80 days is sufficient for this purpose in most cases, this time being essentially the advection time scale for a fluid particle to traverse the model shelf. The same strategy is also used in sensitivity studies as well, although an alternative is to integrate from the steady state conditions of the basic case. It is therefore worth noting that in these sensitivity studies, for most processes, the adjustment time should be considerably less.

Horizontal diffusivities A_M and A_H (for the ocean) are put equal to 250 m^2 s^{-1}, and for the ice, A_D = 1500 m^2 s^{-1} in (16).

3. Results: Simulation of the Bering Sea MIZ

During MIZEX West the wintertime Bering Sea MIZ was studied rather intensively from February to March 1983. Detailed observations of currents, water mass characteristics, wind forcing, and sea ice were made during this period [*Muench and Schumacher*, 1985; *Hendricks et al.*, 1985] (see also *MIZEX Bulletin 6*). The ice edge was close to the shelf break, and the associated oceanic frontal structure was well defined. The data from these observations have been used by *Hendricks et al.* [1985] to estimate the approximate heat balance in the MIZ. These data are also well suited for application of the $x - z$ model described in section 2.

Figure 2 shows the temperature and salinity sections across the Bering Sea MIZ [from *Hendricks et al.*, 1985] taken toward the end of February 1983. Current meter recordings taken during the same winter are, however, less reliable because of biofouling and wave pumping [*Muench and Schumacher*, 1985].

Observations cited by *Hendricks et al.* [1985] suggest that the various parameters take the following approximate values (the uncertainty is as much as 35%) in the wintertime Bering Sea MIZ at the time of observations:

$$U_I(x = L) = -0.2 \pm 0.05 \text{ m s}^{-1}$$

$$D_I(x = L) = 0.5 \pm 0.1 \text{ m}$$

$$A(x = L) = 0.7 \pm 0.1$$

$$T_A = -10 \pm 2°\text{C}$$

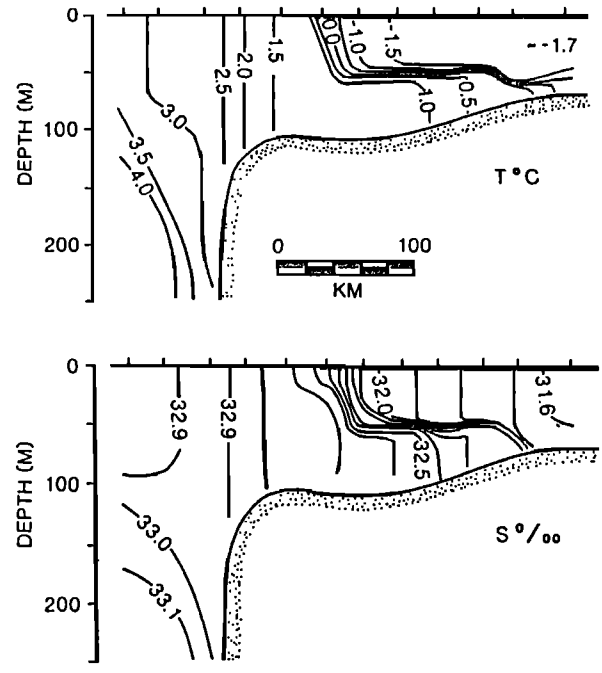

Fig. 2. Observed distributions of temperature (top) and salinity (bottom) along the transect shown in Figure 1 [from *Hendricks et al.*, 1985].

$$U_W = 10 \pm 1.5 \text{ m s}^{-1}$$

$$U(x = 0) = 0.05 \pm 0.02 \text{ m s}^{-1}$$

$$T(x = 0) = 2.5°\text{C}$$

$$S(x = 0) = 32.8 \text{ ppt}$$

U_W is the wind velocity and T_A is the air temperature. It is emphasized that the above estimates can only be used as a first guess in simulating the MIZ conditions corresponding to Figure 2. Our primary objective is to investigate the sensitivity of the MIZ to various factors and therefore gain a better understanding of its variability. It is then necessary to adjust some of these parameters to obtain a simulation that is reasonably close to observations so as to serve as a realistic basic case simulation against which sensitivity studies can be done. Since the wind and the ocean inflow velocities are perhaps the most variable of the forcing parameters, we decided to adjust primarily their values to obtain the basic case simulation.

The sensitivity of the ice edge position and the accompanying circulation became immediately apparent during this exercise. It was also discovered that when we used the value recommended by *Yaglom and Kader* [1974] for the constant b in (17), while the observed mean ice edge position could be obtained by a suitable combination of input parameters, the mixed layer under the ice cover would not cool down to the observed value of −1.7°C but stay consistently 0.2° to 0.3°C higher. Only when we lowered the value of b significantly did we get the observed cooling. We also discovered that tidal mixing was essential. Without it the mixed layer would be too shallow and the two-layer stratification would extend well onto the inner shelf, with the other parameters chosen so as to obtain the proper ice edge position. Also, double-

diffusive convection turned out to be of lesser importance than tidal bottom stirring and other processes.

3.1. *The Basic Case*

The following values were used to obtain the base case simulation:

Wind velocity

$$U_W = 12 \text{ m s}^{-1}$$

Wind angle

$$\alpha_W = 0°$$

Air temperature

$$T_A = -10°\text{C}$$

Inflow velocity

$$U(x = 0) = 0.042 \text{ m s}^{-1}$$

Inflow temperature

$$T(x = 0) = 2.5°\text{C}$$

Drag coefficient

$$C_{DAO} = 2 \times 10^{-3}$$

Drag coefficient

$$C_{DAI} = 3.8 \times 10^{-3}$$

Constant

$$b=0.52$$

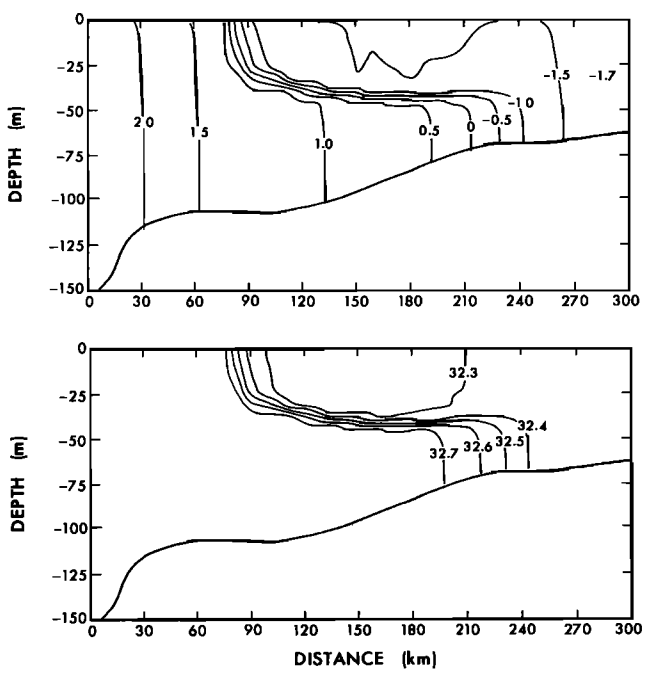

Fig. 3. Distributions of model-simulated temperature (top) and salinity (bottom) fields along the section shown in Figure 1 for the basic case (see the text for forcing conditions). The wind direction is to the left while the flow in the water column is predominantly to the right. Note the strong temperature and salinity front associated with the ice edge, which is located at about 80 km from the offshore boundary. The values are daily averages.

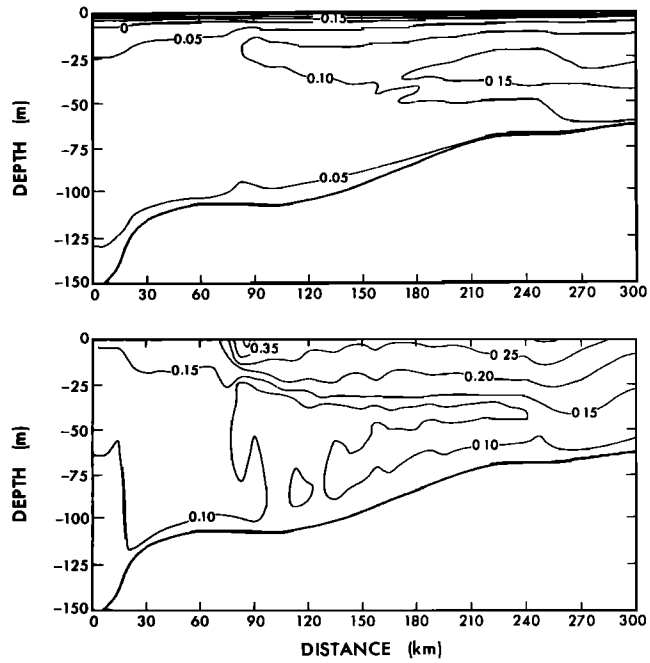

Fig. 4. Distributions of cross-ice-edge (top) and along-ice-edge (bottom) velocities in meters per second for the basic case. Note the thin layer of fluid near the surface that moves in the direction of ice motion, while the rest of the water column moves toward the inner shelf. Note also an along-ice-edge jet at the ice edge, which is located at about 80 km from the offshore boundary. The values are daily averages.

Roughness scale

$$z_0 = 0.02 \text{ m}$$

Cloud fraction is 0.2 and the relative humidity is 0.75.

The simulation corresponds to February 26. Note that the incident solar radiation for the period is not an important factor in the energy balance. The winds are perpendicular to the ice edge and in the off-ice direction. Figures 3–6 show the results. All the quantities displayed henceforth are daily averages at the end of the 80-day run. Note also that because the ice concentration stays well below 80%, the ice internal stresses are an insignificant factor in these simulations.

Figure 3 shows the resulting temperature and salinity distributions. A well-developed two-layer circulation exists under the ice over most of the shelf, while on the inner shelf the water column is well mixed and cools down to −1.7°C, the observed value. The temperature field is somewhat in better agreement with observations (compare Figures 2 and 3) than the salinity structure. The salinities on the inner shelf are overpredicted by about 0.6 ppt, while those on the outer shelf are in somewhat better agreement with observations, which show a significant salinity decrease in the water column approaching the ice edge.

Figure 4 shows the cross-shelf and along-shelf velocity structure. Apart from a thin layer of fluid dragged toward the outer shelf by the winds and ice, the rest of the water column moves toward the inner shelf. A weak along-ice-edge jet with an intensity of about 0.35 m s^{-1} associated with the ice edge front can be seen. Figure 5 shows the turbulence kinetic energy distribution in the water column. Strong mixing occurs both under the ice and in the open water. The two-layer structure under the ice is also evident in these distributions, the bottom layer turbulence being driven primarily by tidal stirring at the bottom. The water column is

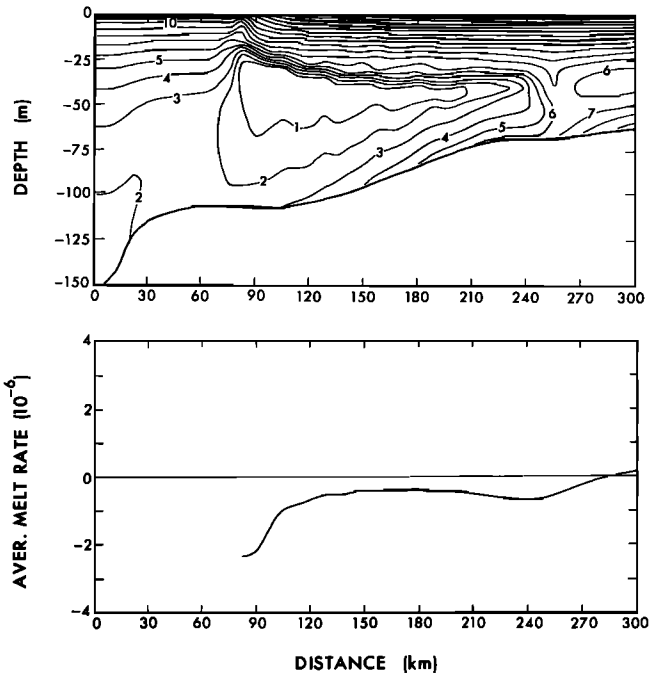

Fig. 5. Distribution of daily average turbulence kinetic energy in cm^2/s^2 (top) and ice melt rate per unit width in meters per second (bottom) for the basic case. Turbulence intensity is high in the upper layers while it is comparatively weaker near the bottom. The melt rate peaks near the ice edge located about 80 km from the offshore boundary.

well mixed on the inner shelf and upstream of the ice edge. Figure 5 also shows the melt rate under the ice across the MIZ. The melt rate shows a characteristic peak near the ice edge but decreases gradually to about one-fifth the peak value over the rest of the MIZ. The total melt rate across the MIZ is about 0.1 m^2 s^{-1} per unit width of the MIZ, consistent with the observed value.

Figure 6 shows the areal fraction A, the average thickness D_I, and the cross-ice-edge velocity of ice. The ice concentration remains more or less uniform across the MIZ before decreasing rapidly to zero at the ice edge. The ice thickness shows a more or less linear decrease across the MIZ, while the ice velocity increases slightly toward the ice edge.

3.2. *Sensitivity Studies*

We now turn to our primary goal, namely the understanding of the variability of the MIZ. We do this by studying the sensitivity of the ice edge to changes in the various forcing variables and model parameters. Table 1 provides a summary of these sensitivity studies along with the basic case.

The position of the ice edge is a sensitive indicator of the overall air-sea momentum and heat flux exchange across the MIZ. For a given influx of ice at the inner shelf, if the parameters are such that the ice melts more rapidly, the ice edge retreats toward the inner shelf; conversely if the melt rate is retarded, it advances toward the outer shelf. Once the warm water moves under the ice, it is separated from the ice by a strong pycnocline. However, the heat for melting the ice comes from both the layer immediately beneath the ice and the bottom layer beneath the pycnocline. Therefore strong turbulence in both layers underneath the ice transfers heat to the vicinity of ice and promotes melting. Conversely, weak mixing leads to slower ice melting. Also, the heat lost by the upper layer to the atmosphere through the leads reduces ice melting because the heat available for melting ice is reduced. This heat loss is a function of the ice concentration and the air-sea temperature difference as well as the wind velocity. Ice concentration is itself a complex function of dynamical and thermodynamic interactions between the ice and the ocean underneath. Thus the rapidity of melting in the MIZ and therefore the position of ice edge on the shelf are complex functions of various processes governing the intensity of mixing and the heat loss through the leads and therefore depend on the parameterization of these processes in the model.

When tides were ignored (Figure 7), the ice edge advanced nearly 80 km. Turbulent mixing in the bottom layer decreased substantially. The absence of this tidal stirring reduces the heat transfer to the upper layer and therefore retards the melting of ice and causes the ice edge to advance. The presence of double diffusion and the shear due to the mean flow over the bottom lead to some transfer of heat across the stable pycnocline, as evidenced by a monotonic decrease in the temperature of the lower layer. When double diffusion was also ignored (not shown), this transfer did not show a substantial further decrease. Therefore tidal mixing appears to be more important than double-diffusive transfer. This is also shown by the simulation in which double diffusion alone was neglected (tidal mixing was retained). The results of this simulation did not differ substantially from the basic simulations (Figure 8). The ice edge advanced less than about 10 km relative to the basic case. It appears therefore that while turbulence due to tidal stirring in the bottom layer is an important factor in the melting of ice, and consequently, the ice edge position, double-diffusive convection is not. *Hendricks et al.* [1985] considered only double-diffusive fluxes in their heat balance estimations and ignored tidal and other mixing effects.

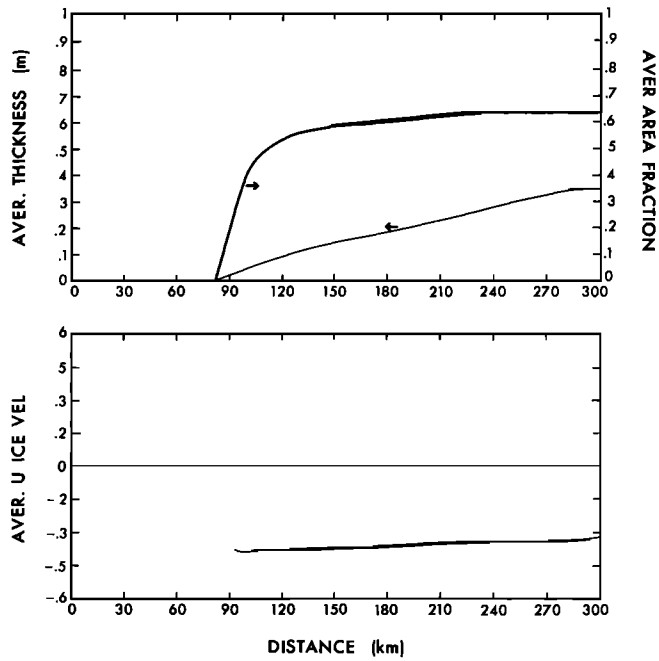

Fig. 6. Distributions of ice concentration and thickness (top) and cross edge ice velocity (bottom) for the basic case. The values are daily averages.

TABLE 1. Parameters for the Series of Runs

Experiment	U_W, m s^{-1}	α_W, deg.	T_A, °C	$U(0)$, m s^{-1}	$T(0)$, °C	U_I, m s^{-1}	z_0, m	b	C_{DAI} × 10^{-3}	Tides	Double Diffusion	Remarks	Figure
1	12	0	−10	0.042	2.5	0.2	0.02	0.52	3.8	Y	Y	basic case	3–6
2										N	Y	tides ignored	7
3										Y	N	DD ignored	8
4								3.14				change in YK	9*a*
5								1.57				coefficient	9*b*
6								0					10
7	14											change in wind	11*a*
8	10											magnitude	11*b*
9		12										change in wind angle	12*a*
10		−12										(+ means to the right)	12*b*
11			−12									change in air	13*a*
12			−8									temperature	13*b*
13					1.5							change in ocean	14*a*
14					3.5							inflow temperature	14*b*
15				0.052								change in ocean	15*a*
16				0.032								inflow velocity	15*b*
17						0.28						change in ice	16*a*
18						0.12						inflow velocity	16*b*
19									2.0			reduced air-ice drag coefficient	17
20							0.01					change in z_0	18*a*
21							0.03						18*b*
22							distribution					Taylor z_0 distribution	19

The parameter b is important to the ice-ocean exchange processes. Figure 9 shows the temperature structure for b = 3.14, the original Yaglom and Kader value. Although it would be possible to adjust other parameters to obtain the observed ice edge position, the temperature structure and the temperature on the inner shelf would not be quite realistic. Figure 9 also shows the temperature structure for b = 1.57; although the simulations are much better, only substantially lower values of b, comparable to that of the base case, appear to yield the correct degree of cooling on the inner shelf. Figure 10 shows the results for b = 0, the case when disparities in the momentum and scalar resistance coefficients are ignored. Clearly a nonzero value of b is essential. However, in view of the uncertainty in the appropriate value for z_0 and other parameters we can only say that the value of b should most likely be comparable to that of the base case. If nothing else, these studies highlight the need for more empirical data on b, either from field observations or, perhaps better, from laboratory experiments which lend themselves to a better control of governing parameters.

Increasing the wind speed to 14 m s^{-1} caused the ice edge to advance more than 80 km, while decreasing it to 10 m s^{-1} made it retreat (see Figure 11). Further decrease to 8 and 6 m s^{-1} did not produce proportionate responses. The advance (and retreat) of the ice edge under increase (and decrease) in wind speed is consistent with observational experience.

A change in the wind angle to the right by 12° caused the ice edge to retreat 80 km, while a shift to the left caused it to

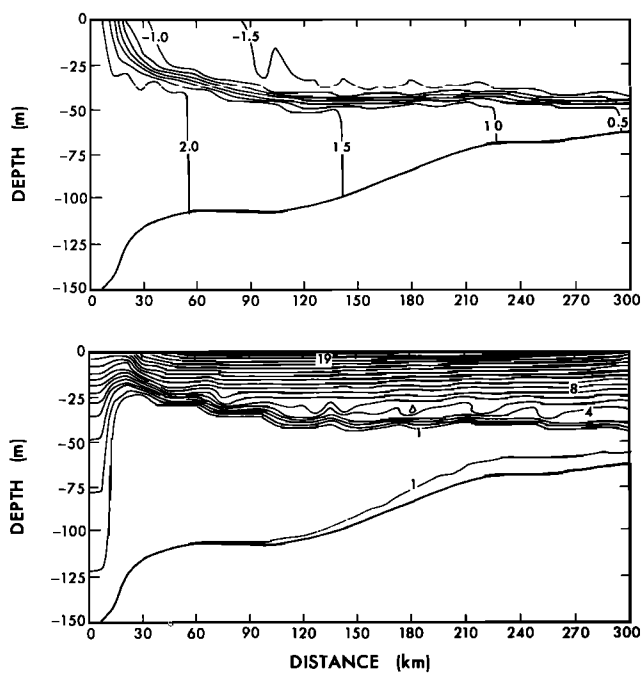

Fig. 7. Distributions of temperature (top) and turbulence kinetic energy in cm^2/s^2 (bottom) when tides are ignored. Note the very weak turbulence in the bottom layer under ice. The ice edge is about 1 km from the offshore boundary.

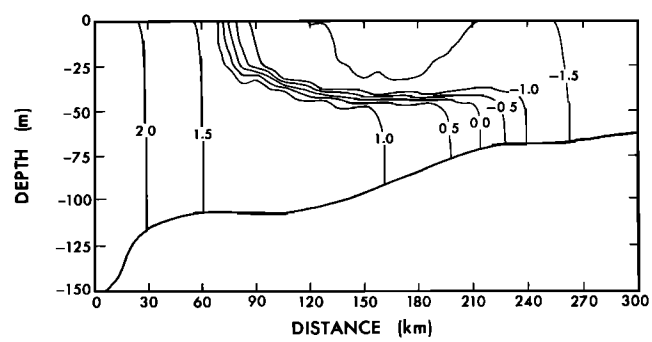

Fig. 8. Daily averaged temperature distributions when only double diffusion is ignored. The relatively weak influence of double diffusion on the ice edge position and therefore the ice melting rate is evident when compared to Figure 3. The ice edge is now located about 70 km from the offshore boundary.

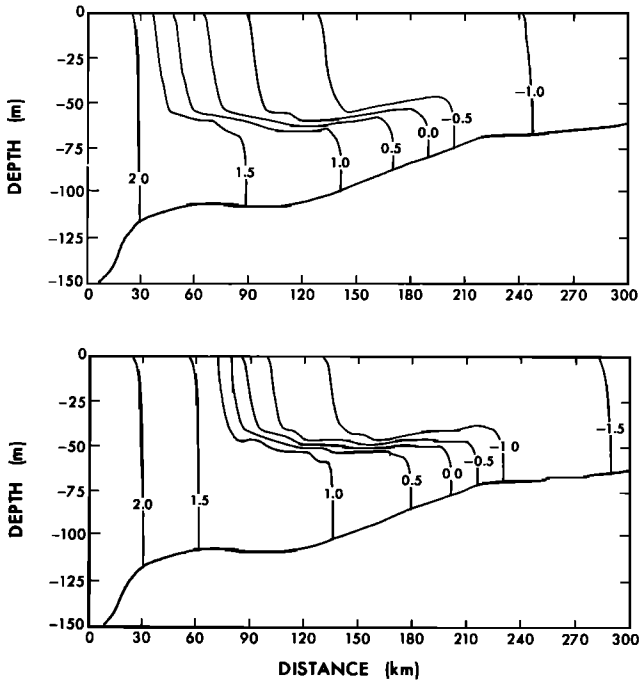

Fig. 9. Temperature distributions as in Figure 3 for b = 3.14 (top) and 1.57 (bottom), where b is the constant in the Yaglom-Kader formulation.

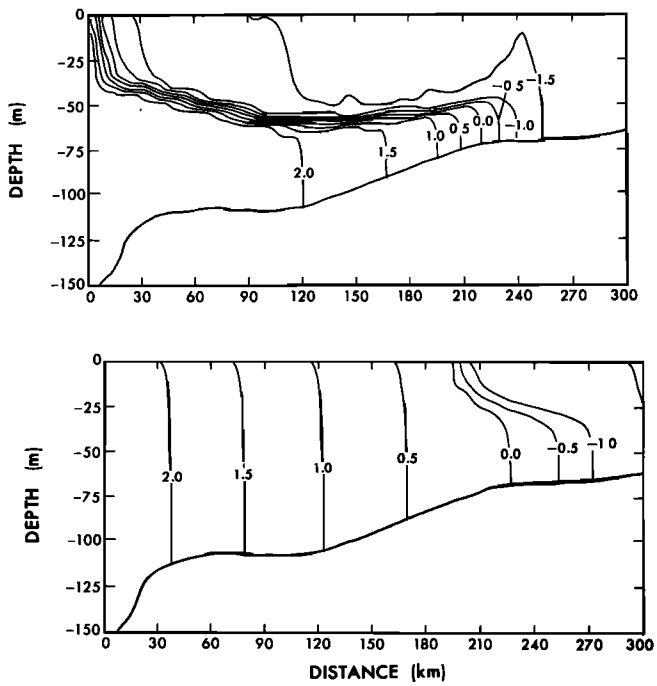

Fig. 11. Sensitivity to wind speed. Temperature fields for wind speeds of 14 m/s (top) and 10 m/s (bottom). The ice edge position can be gleaned from the position of the front. The wind speed is 12 m/s for the basic case.

advance by roughly the same amount (Figure 12). This behavior is related to the cross-ice-edge component of ice velocity, which decreases in the former but increases in the latter cases. The magnitude of the ice velocity remains substantially unchanged.

A change in air temperature also affects the ice edge position (Figure 13). While a decrease in air temperature to −12°C causes the ice edge to advance, an increase to −8°C causes it to retreat by about 80 km. In the former case there is increased heat loss in the leads to the atmosphere so that less heat is available from the upper layer to melt the ice. The ice melting rate is retarded leading to ice edge advance. The reverse happens in the latter case. It appears then that the heat loss in the leads appears to exert an important influence on the position of ice edge on the shelf.

A change in inflow ocean temperature (or velocity) also affects the ice edge position because it affects the amount of heat available for melting the advancing ice (or the cross-

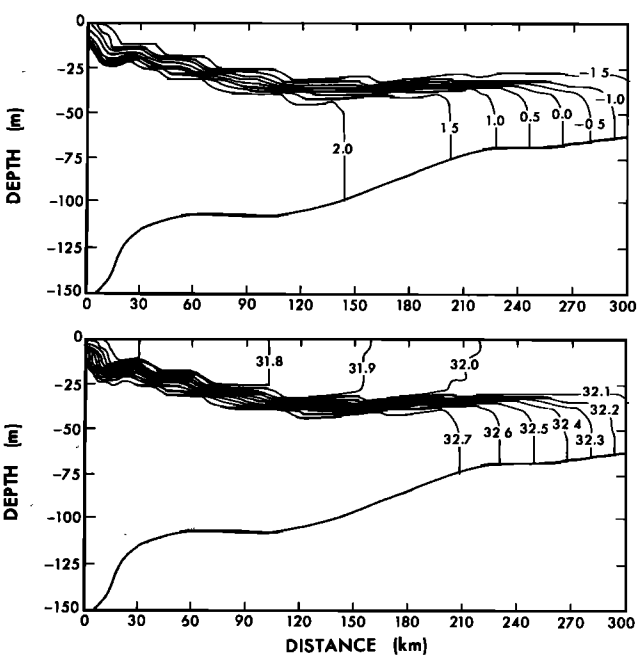

Fig. 10. Temperature and salinity distributions but for b = 0 in the Yaglom-Kader formulation.

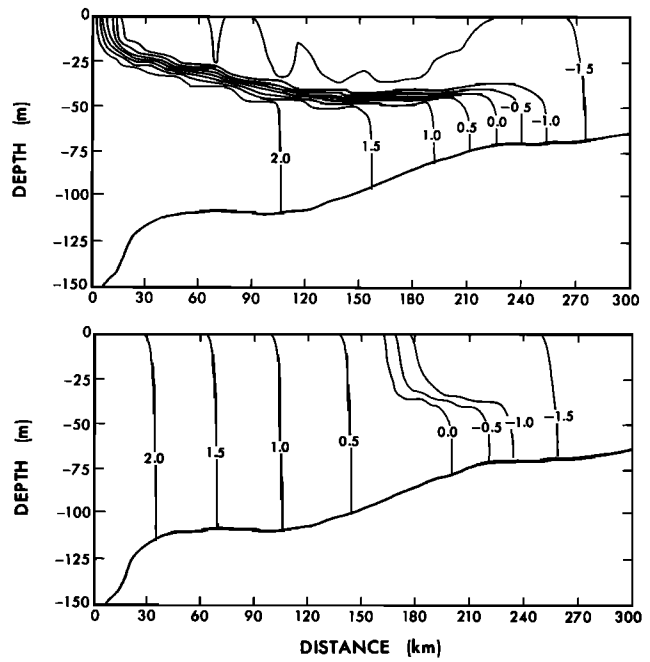

Fig. 12. Sensitivity to wind angle. Temperature fields when the off-ice wind is turned to the right by 12° (top) and to the left by 12° (bottom).

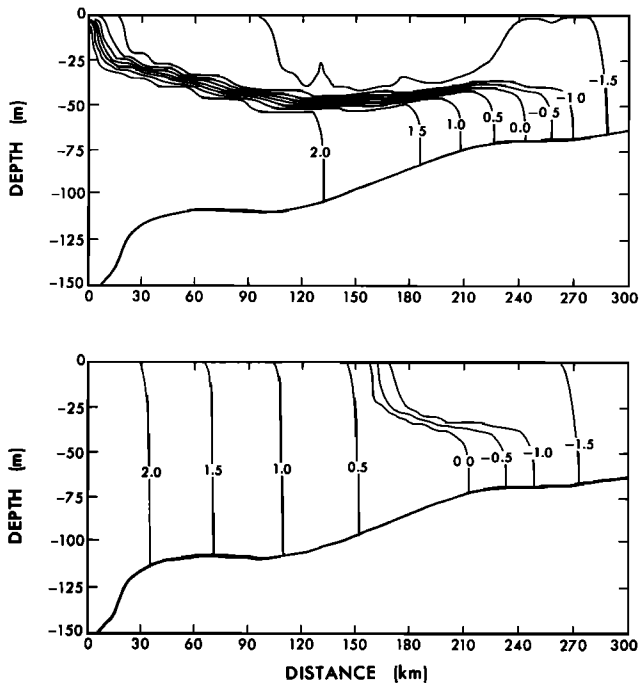

Fig. 13. Sensitivity to air temperature. Temperature distributions for air temperature of −12°C (top) and −8°C (bottom). Air temperature is −10°C for the basic case.

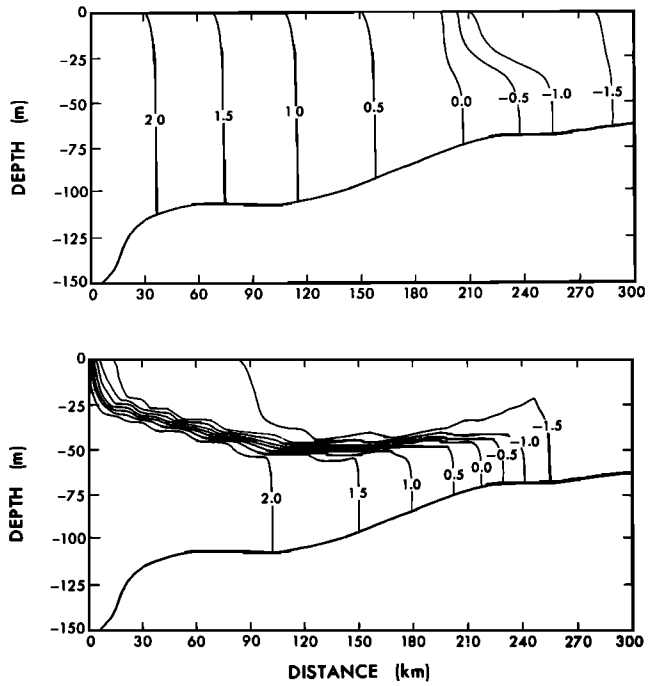

Fig. 15. Sensitivity to water inflow velocity. Temperature distributions for inflow velocity of 0.05 m/s (top) and 0.03 m/s (bottom). For the basic case the value is 0.042 m/s.

ice-edge velocities). Figure 14 shows that a decrease in inflow temperature to +1.5°C causes the ice to advance substantially, while an increase to +3.5°C makes the ice edge retreat about 100 km. Figure 15 shows that an increase in inflow velocity to 0.05 m s^{-1} makes the ice retreat substantially while a decrease to 0.03 m s^{-1} causes the ice edge to advance.

Figure 16 shows the consequences of changing the inflow ice velocity to 0.28 m s^{-1} and 0.12 m s^{-1}. The ice advances 35 km in the former but retreats 25 km in the latter case.

Decreasing the air-ice drag coefficient to the same value as the air-ocean coefficient (0.002) leads to substantially lower air-sea stress and therefore results in much lower ice veloc-

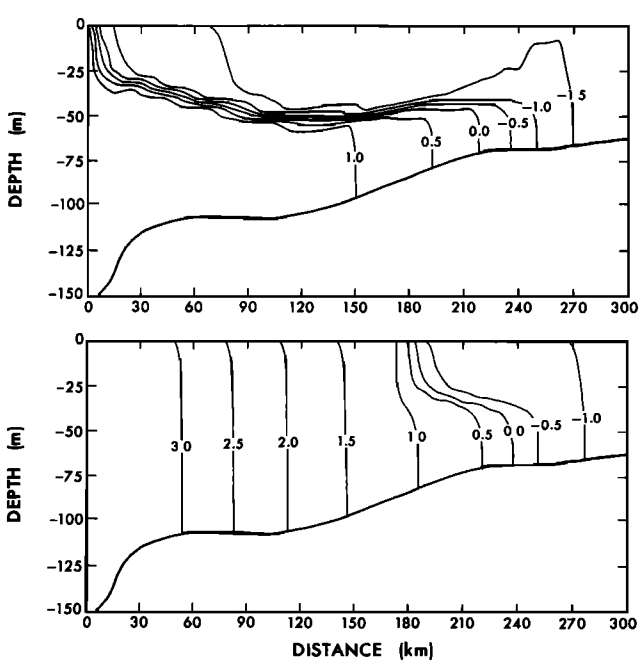

Fig. 14. Sensitivity to inflow water temperature. Temperature fields for inflow temperature of 1.5°C (top) and 3.5°C (bottom). The value for the basic case is 2.5°C.

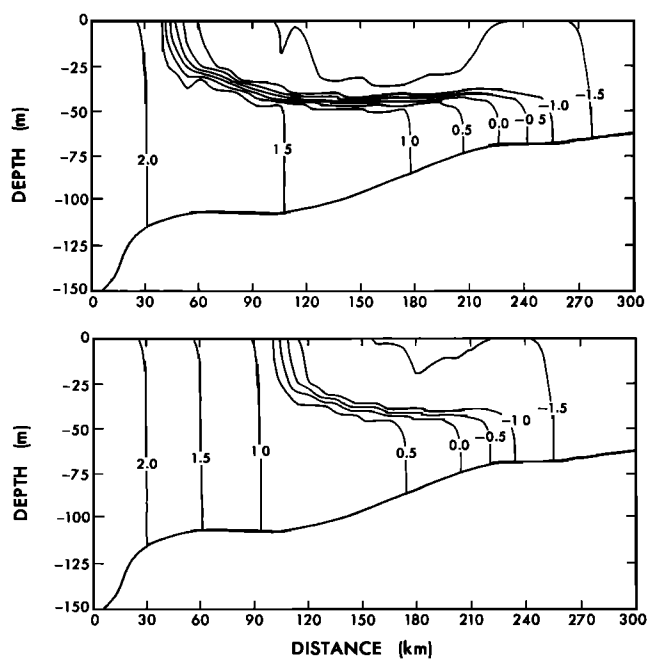

Fig. 16. Sensitivity to ice inflow velocity. Temperature fields for cross edge velocity of 0.28 m/s (top) and 0.12 m/s (bottom). The standard case value is 0.2 m/s.

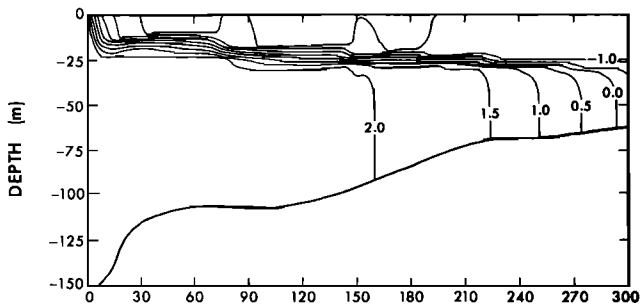

Fig. 17. Temperature distribution when the air-ice drag coefficient is reduced from 0.0038 to 0.002.

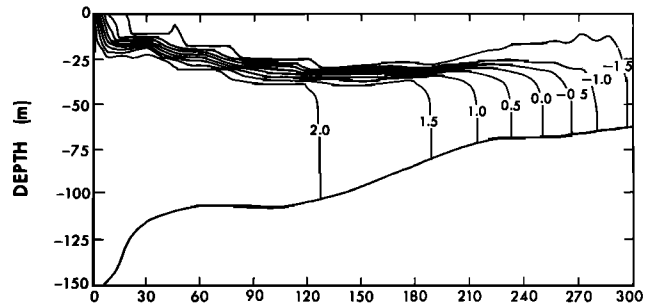

Fig. 19. Temperature distribution when Taylor formulation (z_{0I} = 0.2 m) is used for prescribing the effective momentum roughness scale z_0.

ities. The consequent reduction in mixing causes the ice edge to advance significantly (Figure 17).

A major unknown in modeling MIZ processes is the effective roughness scale (z_0) distribution. We have chosen to use z_0 = 0.02 m, a constant value in these simulations. Obviously, the exact value of z_0 as well as its distribution are important but difficult to estimate with confidence. Figure 18 shows the sensitivity of the results to z_0 = 0.01 and 0.03 m. The average melt rate near the ice edge decreases along with the ice concentration, with decrease in z_0, while the average ice velocity increases and the turbulence level under the ice decreases. The opposite happens with increase in z_0.

Figure 19 shows the resulting temperature structure when z_0 is prescribed according to (19), with z_{0I} = 0.02 m. Since this formulation leads to a decrease in z_0 toward the ice edge, there is a concurrent decrease in the momentum and heat exchanges between the ice and the ocean. The tendency is to retard ice melting, causing the ice edge to advance.

The constant Φ in (10) is the embodiment of our current state of ignorance of the melting and freezing processes in ice-covered oceans; clearly, its value needs refinement.

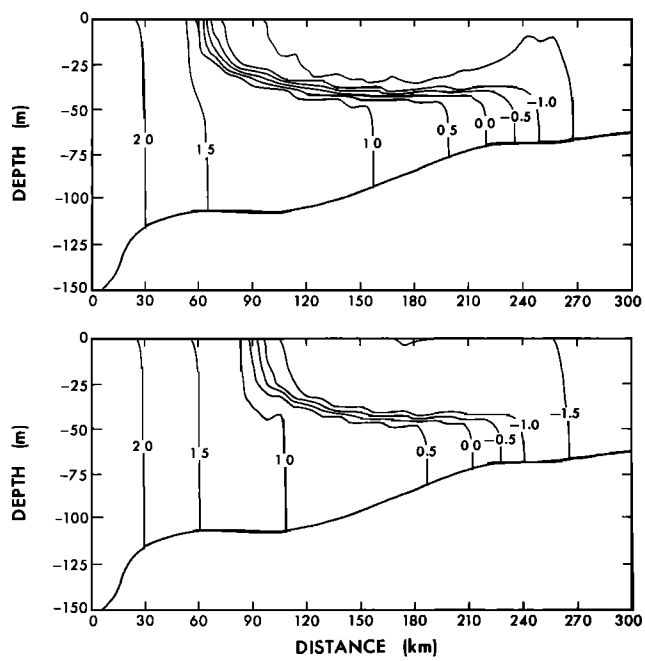

Fig. 18. Sensitivity to the momentum roughness scale z_0. Temperature fields for z_0 = 0.01 m (top) and 0.03 m (bottom). The value for the basic case is 0.02 m.

Sensitivity studies indicate that choosing Φ_M to be 1.0 instead of 0.5 causes the ice edge to retreat substantially (not shown). The value of Φ_M is therefore another important parameter in simulations of ice edge processes (since we are dealing with melting conditions, value of Φ_F is immaterial).

It is clear from the above sensitivity studies that the position of the ice edge and the oceanic structure in the MIZ are rather sensitive to the various parameters affecting the dynamics and thermodynamics of the coupled system. Even small changes in the relevant parameters can cause the steady state position of the ice edge to advance or retreat substantially. Along with the ubiquitous mesoscale activity near the ice edge, this sensitivity of the coupled system may help explain why MIZs are such dynamically active regions.

4. Concluding Remarks

An ice-ocean coupled model has been formulated and a local two-dimensional version applied to simulate the wintertime Bering Sea MIZ. Considering the sensitivity to and the uncertainty in the observational values of the relevant parameters, it is fair to say that the temperature structure underneath the ice, and to some extent the salinities, are reasonably well simulated by the model. The results also indicate that the ice edge position is highly sensitive to parameters affecting the dynamics and thermodynamics of the system. Mixing in both layers under the ice plays an important role in determining the ice edge position. Tidal stirring on the bottom of the shelf appears to be important; double-diffusive transfer across the pycnocline is not.

The thermodynamics of the ice-ocean interaction, especially the formulation of the resistance coefficients for the transfer of heat and salt across a rough ice-sea interface, needs further study. This effort is, however, likely to be hampered by the lack of controlled field and laboratory observations, especially at high values of Schmidt number. Specification of the average momentum roughness scale z_0 in a partially ice-covered ocean also requires further study.

For off-ice winds considered in this paper the precise form utilized for ice internal stresses is immaterial because the ice concentrations in the MIZ seldom become high enough to cause significant internal stresses. But in many other cases, such as during on-ice winds, it will be necessary to pay close attention to ice rheology. The use of a non-Newtonian or viscous-plastic rheology or a suitable blending of both needs to be examined for application to MIZs.

In view of the demonstrated sensitivity of the ice edge position to various forcing parameters, it is not surprising that the MIZs are such dynamically active regions. They are both interesting and challenging to study and to model.

Acknowledgments. This research was supported by the Arctic Programs Branch of the Office of Naval Research under ONR-N00014-84-K-0640. Many thanks to Kalpana Kantha for helping us prepare this manuscript. LHK acknowledges the hospitality and assistance of GFDL in carrying out this work.

REFERENCES

Bennett, T. J., Jr., Atmospheric boundary layer modification in the marginal ice zone, *J. Geophys. Res.*, *91*, 13,033–13,044, 1986.

Dawson, D. A., and O. Trass, Mass transfer at rough surfaces, *Int. J. Heat Mass Transfer*, *15*, 1317–1336, 1972.

Dipprey, D. F., and R. H. Sabersky, Heat and momentum transfer in smooth and rough tubes at various Prandtl numbers, *Int. J. Heat Mass Transfer*, *6*, 329–353, 1963.

Grifoll, J., X. Farrial, and F. Giralt, Mass transfer at smooth and rough surfaces in a circular Couette flow, *Int. J. Heat Mass Transfer*, *29*, 1911–1918, 1986.

Hakkinen, S., Coupled ice-ocean dynamics in the marginal ice zones: Upwelling/downwelling and eddy generation, *J. Geophys. Res.*, *91*, 819–832, 1986*a*.

Hakkinen, S., Ice banding as a response of the coupled ice-ocean system to temporally varying winds, *J. Geophys. Res.*, *91*, 5047–5053, 1986*b*.

Hendricks, P. J., R. D. Muench, and G. R. Stegen, A heat balance for the Bering Sea ice edge, *J. Phys. Oceanogr.*, *15*, 1747–1758, 1985.

Hibler, W. D., III, A dynamic thermodynamic sea ice model, *J. Phys. Oceanogr.*, *9*, 815–846, 1979.

Hibler, W. D., III, and K. Bryan, A diagnostic ice-ocean model, *J. Phys. Oceanogr.*, *17*, 987–1015, 1987.

Hibler, W. D., III, and J. E. Walsh, On modelling seasonal and interannual fluctuations of Arctic sea ice, *J. Phys. Oceanogr.*, *12*, 1514–1523, 1982.

Huppert, H. E., and J. S. Turner, Double-diffusive convection, *J. Fluid Mech.*, *106*, 299–329, 1981.

Ikeda, M., A coupled ice-ocean model of a wind-driven coastal flow, *J. Geophys. Res.*, *90*, 9119–9128, 1985.

Ikeda, M., A mixed layer beneath melting sea ice in the marginal ice zone using a one-dimensional turbulent closure model, *J. Geophys. Res.*, *91*, 5054–5060, 1986.

Josberger, E. G., Bottom ablation and heat transfer coefficients from the 1983 marginal ice zone experiments, *J. Geophys. Res.*, *92*, 7012–7016, 1987.

Kader, B. A., and A. M. Yaglom, Turbulent heat and mass transfer from a wall with parallel roughness ridges, *Int. J. Heat Mass Transfer*, *20*, 345–357, 1977.

Kantha, L. H., Comments on "A heat balance for the Bering Sea ice edge," *J. Phys. Oceanogr.*, *16*, 2205–2207, 1986.

Kantha, L. H., and G. L. Mellor, A numerical model of the atmospheric boundary layer over a marginal ice zone, *J. Geophys. Res.*, *94*, 4959–4970, 1989.

Lepparanta, M., and W. D. Hibler, III, The role of plastic ice interaction in marginal ice zone dynamics, *J. Geophys. Res.*, *90*, 11,899–11,909, 1985.

Marmorino, G. O., and D. R. Caldwell, Heat and salt transport through a diffusive thermohaline interface, *Deep Sea Res.*, *23*, 59–67, 1976.

Maykut, G. A., and D. K. Perovich, The role of shortwave radiation in the summer decay of a sea ice cover, *J. Geophys. Res.*, *92*, 7032–7044, 1987.

McPhee, M. G., G. A. Maykut, and J. H. Morrison, Dynamics and thermodynamics of the ice/upper ocean system in the marginal ice zone of the Greenland Sea, *J. Geophys. Res.*, *92*, 7017–7031, 1987.

Mellor, G. L., and L. H. Kantha, An ice-ocean coupled model, *J. Geophys. Res.*, this issue.

Mellor, G. L., and T. Yamada, Development of a turbulence closure model for geophysical fluid problems, *Rev. Geophys.*, *20*, 851–875, 1982.

Mellor, G. L., M. G. McPhee, and M. Steele, Ice-seawater turbulent boundary layer interaction with melting or freezing, *J. Phys. Oceanogr.*, *16*, 1829–1846, 1986.

MIZEX Bulletin 6, Spec. Rep. 85-6, U.S. Army Cold Reg. Res. Eng. Lab., Hanover, N. H., 1985.

Mofjeld, H. O., Observed tides on the northeastern Bering Sea shelf, *J. Geophys. Res.*, *91*, 2593–2606, 1986.

Muench, R. D., and J. D. Schumacher, On the Bering Sea ice edge front, *J. Geophys. Res.*, *90*, 3185–3197, 1985.

Orlanski, I., A simple boundary condition for unbounded hyperbolic flows, *J. Comput. Phys.*, *21*, 251–269, 1976.

Overland, J. E., Atmospheric boundary layer structure and drag coefficients over sea ice, *J. Geophys. Res.*, *90*, 9029–9049, 1985.

Overland, J. E., and C. H. Pease, Modeling ice dynamics of coastal seas, *J. Geophys. Res.*, *93*, 15,169–15,637, 1988.

Overland, J. E., R. M. Reynolds, and C. H. Pease, A model of the atmospheric boundary layer over the marginal ice zone, *J. Geophys. Res.*, *88*, 2836–2840, 1983.

Owen, P. R., and W. R. Thompson, Heat transfer across rough surfaces, *J. Fluid Mech.*, *15*, 321–334, 1963.

Parkinson, C. L., and W. M. Washington, A large-scale numerical model of sea ice, *J. Geophys. Res.*, *84*, 311–337, 1979.

Reynolds, M., On the local meteorology at the marginal ice zone of the Bering Sea, *J. Geophys. Res.*, *89*, 6515–6524, 1984.

Roed, L. P., A thermodynamic coupled ice-ocean model of the marginal ice zone, *J. Phys. Oceanogr.*, *14*, 1921–1929, 1984.

Roed, L. P., and J. J. O'Brien, A coupled ice-ocean model of upwelling in the marginal ice zone, *J. Geophys. Res.*, *88*, 2863–2872, 1983.

Rood, R. B., Numerical advection algorithms and their role in atmospheric transport and chemistry models, *Rev. Geophys.*, *25*, 71–100, 1987.

Semtner, A. J., Jr., Numerical simulation of the Arctic Ocean circulation, *J. Phys. Oceanogr.*, *6*, 409–425, 1976.

Semtner, A. J., Jr., A numerical study of sea ice and ocean circulation in the Arctic, *J. Phys. Oceanogr.*, *17*, 1077–1099, 1987.

Shen, H. H., W. D. Hibler, III, and M. Lepparanta, The role of floe collisions in sea ice rheology, *J. Geophys. Res.*, *92*, 7085–7096, 1987.

Sheppard, P. A., Transfer across the Earth's surface and through the air above, *Q. J. R. Meteorol. Soc.*, *84*, 205–224, 1958.

Smedstad, O. M., and L. P. Roed, A coupled ice-ocean model of ice breakup and banding in the marginal ice zone, *J. Geophys. Res.*, *90*, 876–882, 1985.

Steele, M., G. L. Mellor, and M. G. McPhee, The role of the molecular sublayer in the melting or freezing of sea ice, *J. Phys. Oceanogr.*, *19*, 139–147, 1989.

Takao, S., and U. Narusawa, An experimental study of heat and mass transfer across a diffusive interface, *Int. J. Heat Mass Transfer*, *23*, 1283–1285, 1980.

Taylor, P. A., Comments and further analysis on effective roughness lengths for use in numerical three-dimensional models, *Boundary Layer Meteorol.*, *39*, 403–418, 1987.

Turner, J. S., Multicomponent convection, *Annu. Rev. Fluid Mech.*, *17*, 11–44, 1985.

Yaglom, A. M., and B. A. Kader, Heat and mass transfer between a rough wall and turbulent fluid flow at high Reynolds and Peclet numbers, *J. Fluid Mech.*, *62*, 601–623, 1974.

L. H. Kantha, Institute for Naval Oceanography, Stennis Space Center, MS 39529.

G. L. Mellor, Atmospheric and Oceanic Sciences Program, Princeton University, James Forrestal Campus, P. O. Box 308, Princeton, NJ 08542.

(Received June 6, 1988;
accepted October 27, 1988.)